Int. J. Environ. Res., 7(2):407-422, Spring 2013
ISSN: 1735-6865

Sensitivity Analysis of METRIC–Based Evapotranspiration Algorithm

Mokhtari, M. H. [1&a], Ahmad, B.[2*], Hoveidi, H.[3] , Busu, I.[2]

[1]Department of Remote Sensing, Faculty of Geo-information science and engineering, University Technology of Malaysia (UTM), Malaysia
[a] Faculty of natural resources, Yazd University, Yazd, Iran

[2] Department of Remote Sensing, Faculty of Geo-information science and engineering, University Technology of Malaysia (UTM), Malaysia

[3]Graduate faculty of Environment, University of Tehran, Tehran, Iran

[2]Department of Remote Sensing, Faculty of Geo-information science and engineering, University Technology of Malaysia (UTM), Malaysia

Received 26 Feb. 2012; Revised 8 Aug. 2012; Accepted 25 Aug. 2012

ABSTRACT: METRIC (Mapping Evapotranspiration at High Resolution with Internalized Calibration) is known as an appropriate surface energy balance model for the estimation of the spatial distribution of evapotranspiration (ET) in semi-arid regions. Based on lysimeter measurements, METRIC has shown ET estimates of 10% on a sub-field scale on a daily basis. There is a need to identify how the model is sensitive to the input parameters. Therefore, the most influential parameters in the algorithm can be identified and the model can be further improved. Sensitivity analysis at three levels of vegetation cover shows that METRIC is highly sensitive to dT, surface temperature, net radiation, sensible heat flux, surface albedo, soil heat flux, and air temperature. It is also moderately sensitive to friction velocity, aerodynamic resistance to heat transfer, surface emissivity and less sensitive to leaf area index, soil adjusted vegetation index, wind speed(except wind speed at low level of vegetation cover)', and roughness length for momentum (except Z_{om}<0.1). A two-factor analysis of the algorithm's primary inputs showed that the pair albedo-surface temperature is the most and the normalized vegetation index-soil adjusted vegetation index or normalized vegetation index-leaf area index is the least effective pair in this model. In order to improve the accuracy of METRIC, this study suggests upgrading the equations for the above-mentioned effective variables.

Keywords: Evapotranspiration, METRIC, Pistachio, Semi-Arid, Sensitivity Analysis

INTRODUCTION

An accurate estimation of evapotranspiration (ET) is essential for the determination of actual plant water requirements and water resource planning and management water and water saving, especially in arid and semi-arid regions where water resources are scarce and economic production depends on irrigation. Effective water management is a main component of a successful water conservation plan (Mondéjar-Jiménez *et al.,* 2011; Ferrari *et al.,* 2010). In this area water shortage and drought are the major environmental concern (Lin *et al.,* 2011) and as a result precise information concerning spatial variation and periodic information of ET (Irmak and Kamble, 2009), that are nowadays easy for access independently on a pixel basis by means of satellite data is necessary (Ramos *et al.,* 2009). Recently, various satellite-based models such as Empirical direct method, inference method, residual method, and deterministic method have been developed to quantify the spatial variation of ET (Choi *et al.,* 2009). Nevertheless, it is complicated to find a balance between parameterization requirements and model accuracy. Mapping Evapotranspiration at high Resolution with Internalized Calibration (METRIC), as a variant of SEBAL (Surface Energy Balance for Land) developed by Bastiaanssen (1995), estimates the spatial distribution of actual ET from the residual part of the energy budget at the earth surface. METRIC has been identified as an accurate and relatively cost-effective ET model (Allen and Bastiaanssen, 2005; Chavez *et al.,* 2009; Conrad *et al.,* 2007; Folhes *et al.,* 2009; Hendrickx *et al.,* 2007; Tasumi et al., 2005b; Trezza, 2006) specially for the advective conditions in semi-arid regions. This is because reference ET

*Corresponding author E-mail:baharinahmad@utm.my

(ET_{ref}) calculated through ASCE-EWRI standardized Penman-Monteith is used to convert an instantaneous value into a daily basis or a higher time level instead of evaporative fraction by SEBAL (Allen *et al.,* 2007b; Allen *et al.,* 2005). Thus, the conversion is better incorporated by taking into account the daily climatic variability. To estimate ET, most energy balance models require surface temperature, calculated from thermal infrared radiance data. METRIC and SEBAL utilize satellite data with recorded radiation in the visible, near-infrared and thermal infrared parts of the electromagnetic spectrum in separate spectral bands. Both models use the same procedure to determine the near surface temperature gradient (dT) instead of the absolute surface temperature. Consequently, there is no need for the absolute aerodynamic surface temperature and air temperature. METRIC is internally calibrated in two extreme conditions, namely wet and dry pixels, using an hourly alfalfa reference ET calculated from weather data (Allen *et al.,* 2007b). In addition, the internal calibration of sensible heat and surface temperature gradient eliminates the atmospheric correction of surface temperature and albedo (Tasumi *et al.,* 2005b).

The model requires wind speed (Ws), air temperature air-t, hourly ET_{ref} calculated from ASCE-EWRI standardized Penman-Monteith method as well as satellite data containing visible-near infrared, shortwave and thermal-infrared band(s) (Folhes *et al.,* 2009). From the input satellite and weather data, primary outputs including NDVI (Normalized vegetation Index), LAI (Leaf Area Index), SAVI (Soil Adjusted Vegetation Index), and surface albedo are estimated. Subsequently, the primary parameters are used to calculate energy balance components as well as the latent energy utilized by ET at the satellite overpass time.

SEBAL has been applied in more than 30 countries with different climatic conditions, and the accuracy of the model is reported to be from 67% to 95% for instantaneous ET and 70% to 98% on a daily basis in previous studies (Bastiaanssen *et al.,* 2005). In addition, based on the lysimeter measurement, METRIC model showed ET estimates within 10% on a sub-field scale on daily, monthly and annual bases (Allen *et al.,* 2005). Moreover, the errors of 14.7%, 8.1%, 1.5% and -7.4% were reported by comparing ET from Soil Water Balance (SWB) method to METRIC estimate over different crop types and irrigation managements (Chavez *et al.,* 2007). Although previous studies are found satisfactory, the applicability of the model under a variety of crops and climatic conditions as well as sources of errors has been recommended to be investigated (Gowda *et al.,* 2008). The errors can be reduced by identifying critical parameters and equation in an algorithm through an appropriate sensitivity analysis. Sensitivity analysis is known as an important procedure to determine the model behavior that is developed for further application (Nakane and Haidary, 2010). In order to identify the most influential input parameters of the SEBAL that cause significant uncertainty in model few numbers of researches have been conducted in the last. The effect of input parameters on SEBAL output has been studied by several authors. Sensible heat flux as a component of energy balance equation was found to be most sensitive that utilize two reference points namely hot and cold pixels for calculation. Therefore, appropriate selection of hot and cold pixels has been suggested (e.g. in SEBAL, METRIC models) for accurate estimation of ET (Timmermans *et al.,* 2007; Long *et al.,* 2011; Bastiaanssen, 1995; Wang *et al.,* 2009). The standard deviation of H estimates from SEBAL using high spatial resolution data was reported to be smaller than that using low spatial resolution data (Long *et al.,* 2011). Moreover, different vegetation covers have different effects on soil and canopy temperature estimation (Wang *et al.,* 2009; Timmermans *et al.,* 2007; Long *et al.,* 2011). The effects of spatial resolution on SEBAL ET can also be found in the study by Long, et al. (2011). Nevertheless, previous studies performed single inputs sensitivity analysis or they evaluated the effect of input on sensible heat flux estimation (Timmermans *et al.,* 2007; Long *et al.,* 2011). It should be noted that in energy balance model, ET is estimated by subtracting soil heat and sensible heat from the net radiation. Therefore, the errors in calculation of each component must be taken into account. This study evaluates two-factor sensitivity analysis in addition to the single primary and intermediate input sensitivity analysis. Two-factor analysis is important when calculation of an input is based on another.

The present study applies METRIC model with a LANDSAT TM5 image to a pistachio field in a semi-arid region to estimate the actual daily ET. Then, as its main objective, the study verifies how METRIC is sensitive to the input variable and equations by analyzing the sensitivity of the algorithm. Moreover, the most dominant parameter(s) is/are determined. As a result, the algorithm can be improved by upgrading the most influential parameters and equations in the model.

MATERIALS & METHODS

The study was conducted in a pistachio fields located in the south-west of Yazd, Iran, somewhere within 31.28 and 31.48 N and 54.80 and 55.00 E (fig.1). The tree spacing is 6 m $\times$ 1.7 m and, during the growing season the soil surface is maintained free of weeds by periodic tillage. The soil types in the experimental site

are mainly sandy loam at the top 10 cm and clay loam bellow this depth. Irrigation water resources used to be groundwater in this area, and it is impossible to have economical crop production without a reliable irrigation system. The irrigation method is traditional flooding with the frequency of 30 to 35 days which is decreased to 40 to 45 days during autumn and winter months. According to De-Marton climatic classification method, the area has a predominantly arid or semi-arid desert climate. The average annual rainfall in the study area is about 71.9 mm that mostly occurs in winter months. Based on the 10-year weather data recorded at the Meteorological Organization in the city of Yazd, the monthly evaporation and the mean air relative humidity are about 264 mm and 25% respectively.

Path/row 161-38 LANDSAT TM5 data acquired on 17 July 2010 were obtained from USGS Global Visualization Viewer (GLOVIS, http://glovis.usgs.gov). The weather data including wind speed, air temperature, radiation, humidity, and dew point recorded in ten-minute intervals at a weather station nearby the study area were used as the input for METRIC model as well as ASCE Penman–Monteith to estimate the alfalfa reference evapotranspiration. One or two weather conditions are proposed to be enough to calculate the reference ET for a LANDSAT image that covers 180 by 180 km (Allen *et al*., 2007b). However, this study utilized the weather data from the only available weather station located almost in the middle of the pistachio field.

The geometric correction of the image was performed by collecting 20 well-distributed ground control points (GCPs). First, order polynomial transformation with a nearest neighbor resampling method was applied to each image to fit the image coordinate to the coordinate of the ground control points. The accuracy of geo-referencing was evaluated by calculating the Root Mean Square Error (RMSE) which yielded less than half size of the original pixel. Then, a subset of the area of interest was generated from the image scenes. Radiometric and atmospheric calibration was performed by converting the original digital numbers to radiance using Equation. 1 (Chavez, 1988).

$$L = gain * DN + offset \quad (1)$$

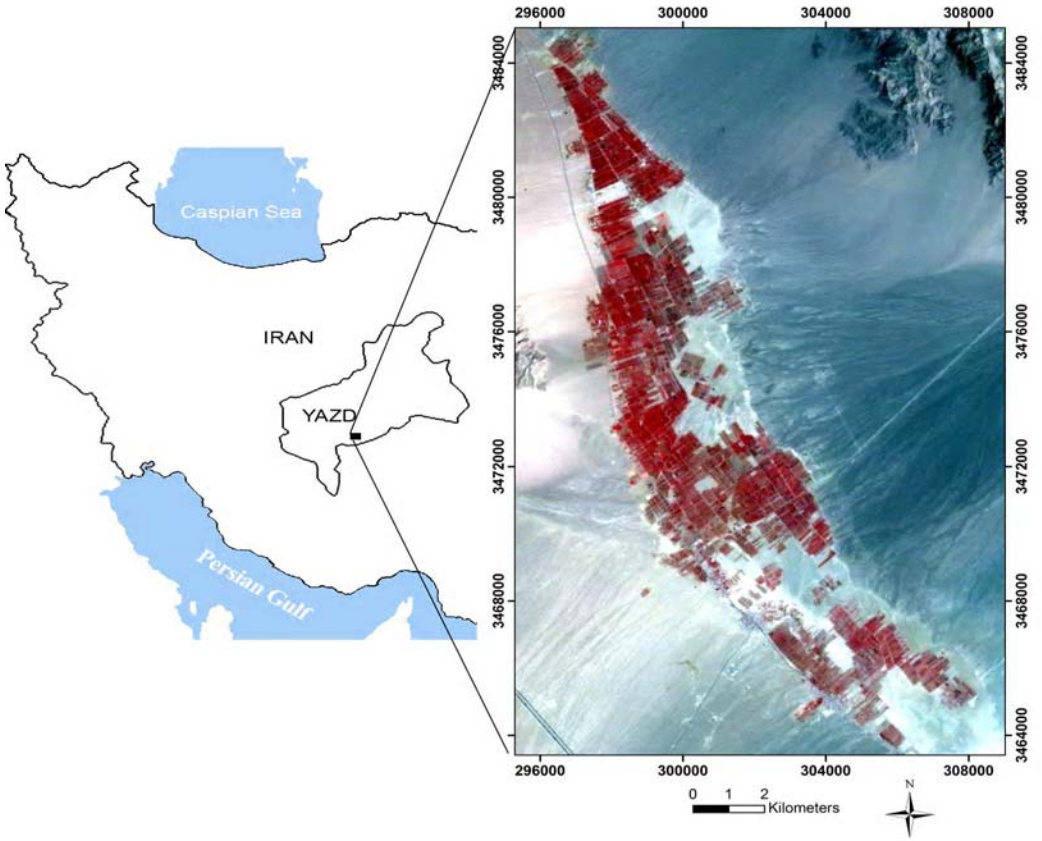

Fig. 1. Location of the study area, LANDSAT FCC of 4,3,2 (Right)

where L is the radiance ($Wm^{-2}str\mu m$), and DN is the radiometric value or the digital number. The gain is calculated by the following equation (Markham and Barker, 1986).

$$gain = \frac{L_{\max} - L_{\min}}{255} \quad (2)$$

where $L_{\max}$ and $L_{\min}$ are the upper radiance limit and the lower radiance limit respectively. They are provided by an image supplier and can be found on the metadata of each dataset. To convert the radiance values into the top-of-atmosphere reflectance of visible-near infrared and short waves bands, the following equation was used (Allen *et al.*, 2007b):

$$\rho = \frac{L_\lambda \Pi d^2}{ESUN_\lambda \cos\theta} \quad (3)$$

where $ESUN_\lambda$ is the band dependence exoatmospheric irradiance (Chander and Markham, 2003), ($Wm^{-2}str\mu m$), θ is the solar zenith angle, and d is the earth-sun distance (AU). In order to correct the top-of-atmosphere reflectance image for scattering and absorption of incoming and outgoing, near surface vapor pressure-based atmospheric correction was employed to convert the top-of-atmosphere reflectance into at-surface-reflectance (Tasumi *et al.*, 2005b; Gowda *et al.*, 2008). Following the method by Allen, et al.(2007b), three stages were devised to convert the DN values of the thermal band to the surface temperature. First, DNs were converted into radiance. Then, the thermal band radiances were converted into corrected radiance. Finally, Equation 4 was used to calculate the surface temperature from the corrected radiance, two constant values (K_1 and K_2), and narrow-band emissivity. Calculating narrow-band emissivity requires the estimation of narrow-band transmissivity that, in this study, was obtained from the method of MODTRAN-based atmospheric radiation transfer simulation for clear sky (Allen *et al.*, 2007b). Detailed information about the radiometric calibration and estimation of surface temperature from LANDSAT data can be found in Chander and Markham, (2003).

$$T_s = \frac{K_2}{\ln\left((\varepsilon_{NB}\frac{K_1}{Rad_{b6}})+1\right)} \quad (4)$$

where K_1=607.76 and K_2=1260.56 ($Wm^{-2}sr^{-1}\mu m^{-1}$) are two constant values, Rad_{b6} is the corrected thermal radiance calculated from the spectral radiance of band 6 of LANDSAT image, and ε_{NB} is the narrow-band emissivity (an empirical equations were also presented by Bastiaanssen et al. (2002)).

An energy balance model is employed to calculate the instantaneous latent heat loss (LE) Wm^{-2} at the earth's surface on a pixel-by-pixel basis at the satellite overpass time. The general equation is given as follows:

$$LE = R_n - G - H \quad (5)$$

where LE is the instantaneous latent heat loss (Wm^{-2}) utilized for evapotranspiration. It is calculated as a residual of the energy budget. LE can be converted to an hourly or daily ET by dividing it by the latent heat of vaporization (Chavez *et al.*, 2009). R_n(Wm^{-2}) is the net solar radiation (the balance of incoming and outgoing short waves and long-wave radiation at the surface), G (Wm^{-2}) is the soil heat flux conducted into soil, and H (Wm^{-2}) is the sensible heat flux convected into the air. A similar approach is used to calculate R_n and G by SEBAL and METRIC. Net radiation is partitioned into the incoming shortwave radiation originated from the sun, the outgoing short waves (a fraction of which is reflected by the earth surface), the incoming long-wave radiation originated from the atmosphere, and the outgoing long-wave radiation emitted by the earth surface (Walter *et al.*, 2002):

$$R_n = R_{S\downarrow} - \alpha R_{S\downarrow} + R_{L\downarrow} - R_{L\uparrow} - (1-\varepsilon_o)R_{L\downarrow} \quad (6)$$

where R_n is the net radiation, α is the surface albedo that is calculated by integrating satellite spectral reflectance values from bands 1–5 and 7 of LANDSAT image using weighing function (Tasumi *et al.*, 2007). Also, $R_{S\downarrow}$ (Wm^{-2}) is the incoming solar radiation measured at the local weather station or as a constant value estimated at the satellite overpass time (Eq. 7) (Allen *et al.*, 2007b).R_L and R_L(Wm^{-2}) are the incoming and the outgoing long-wave radiations respectively. is the broadband surface thermal emissivity that is calculated as a function of Leaf Area Index (LAI) or Normalized Difference Vegetation Index (NDVI) as indicated in Eq.15 (Tasumi, 2003). The term $(1-\varepsilon_o)R_{L\downarrow}$ represents the fraction of the incoming long- wave radiation reflected from the surface. Note the following equation now:

$$R_{S\downarrow} = \frac{G_{sc} COS\theta_{rel} \tau_{sw}}{d^2} \quad (7)$$

where θ_{rel} is the solar incidence, G_{sc} serves as the so const (1367 Wm-2),d^2 is the relative Earth–Sun distance squared, $\tau_{sw}$and stands for the broad-band atmospheric transmissivity.

The outgoing long-wave ($R_{L\uparrow}$) component of the energy balance equation is calculated as a function of surface emissivity and surface temperature using Stephan-Boltzman equation:

$$R_{L\uparrow} = \varepsilon_o \sigma T_s^4 \quad (8)$$

where σ is the Stephan-Boltzman constant ($5.67 * 10^{-8} Wm^{-2} K^{-4}$), $\varepsilon_o$is the surface emissivity, is T_s the surface temperature (k) that, in case of using LANDSAT image, is calculated from the radiance values of band 6 (Eq. 4)

The surface emissivity is proposed to be calculated from the leaf area index in METRIC as the following:

$$\varepsilon_o = 0.95 + 0.01 * LAI \quad (9)$$

The equation above was used to calculate ε_o where LAI was found to be lower than 3 and was set to 0.98 for the area with LAI higher than 3 (Tasumi, 2003).

The thermal radiation emitted by the atmosphere reaches the earth surface and is considered as the incoming long-wave radiation.R_L is calculated using Stephan-Boltzman equation as follows:

$$R_{L\downarrow} = \varepsilon_a \sigma T_a^4 \quad (10)$$

where ε_a is the air emissivity calculated through an empirical equation (Eq. 11) (Bastiaanssen *et al.*, 1998),σ is the Stephan-Boltzman constant ($5.67 * 10^{-8} Wm^{-2} K^{-4}$), and T_a is the air temperature in Kelvin that has been measured at the weather station nearby the study area.

$$\varepsilon_a = 0.85(-LN\tau_{sw})^{0.09} \quad (11)$$

where $\tau_{sw}$is the atmospheric transmissivity.

LAI is an indicator of the canopy resistant to vapor flux. It is defined as the ratio of the total area of one side of plant leaves to the unit of ground area. LAI was measured on the ground at different levels by utilizing LI-COR, LAI2000 instrument and GPS. The measurements were plotted against the SAVI values estimated through LANDSAT spectral bands (Eq.13). An exponential equation was developed on the basis of the relationship between SAVI and the corresponding LAI values measured on the ground (Eq.12). The standard error and the correlation coefficient of this equation were 0.678 and 0.977 respectively. In addition, LAI was set to zero where SAVI was less than 0.065 based on the ground control points.

$$LAI = 21.202 * SAVI^2 - 2.905 * SAVI + 2.948 \quad (12)$$

where SAVI is the Soil Adjusted Vegetation Index estimated through the equation proposed by Allen et al. (2007a):

$$SAVI = \frac{(1+L)(\rho_4 - \rho_3)}{L + (\rho_4 + \rho_3)} \quad (13)$$

where L is the soil-brightness dependent correction factor that is calculated by soil-vegetation line slop created by plotting the near infrared and the red bands (Allen *et al.*, 2007a). Therefore, when L is set to zero, SAVI becomes equal to NDVI.

The amount of energy conducted into soil is referred to as soil heat flux (G). An empirical equation is used by METRIC to estimate soil heat flux (Bastiaanssen, 2000).

$$G = (T_S - 273.15)(0.0038 + 0.0074\alpha)(1 - 0.98 NDVI^4) R_n \quad (14)$$

where T_s is the surface temperature in Kelvin using a thermal band, α is the surface albedo, and NDVI is the vegetation index calculated from red and near-infra red spectral bands. In case of using LANDSAT data, bands 3 and 4 are used to calculate NDVI:

$$NDVI = \frac{\alpha_4 - \alpha_3}{\alpha_4 + \alpha_3} \quad (15)$$

where α_4 and α_3 are the reflectance data of bands 4 and 3 respectively.

The ratio of heat loss into the air through convection due to temperature differences is known as sensible heat flux (H). It can be predicted from the difference between the surface aerodynamic temperature and a reference height air temperature (Brutsaert, 1982).

In both METRIC and SEBAL, the aerodynamic temperature gradient-based equation (Eq. 17) for heat transport is estimated by calculating the temperature difference between the two near surface heights.

$$H = \rho C_p \frac{dT}{r_{ah}} \quad (16)$$

where $\rho$is the air density kgm^{-3}, C_p is the air specific heat at a constant pressure (≈1004 $Jkg^{-1}k^{-1}$), dT (K) is the near surface temperature difference between the two near surface heights, and r_{ah}(*sm-1*) is the aerodynamic resistance to heat transfer (between the two near surface heights, 0.1 and 2m) that is calculated

by extrapolating wind speed to some blending heights above the ground surface (100 to 200 m) and correcting the iterative stability based on Monin-Obukhov function. In Eq. 16, both $r_{ah}$and dT are unknown. Therefore, first is calculated for the neutral stability as:

$$r_{ah} = \frac{LN(z_2 / z_1)}{u^* k} \quad (17)$$

where Z_1 and $Z_2$are the heights above zero plane displacement height of vegetation that is set to 0.1 m for each pixel, z_2 is the reference height just above the plant canopy set to 2 m, $u^*(ms^{-1})$ is the friction velocity calculated from the logarithmic wind law for neutral atmospheric conditions, and K is Von Karman's constant equal to 0.41.

Then, using equation (18) and (20), $u^*$and u_{200} are calculated for the neutral atmospheric condition at the weather station:

$$u^* = \frac{ku_{200}}{LN(200 / zom)} \quad (18)$$

where U_{200} is the wind speed at the blending height (200m, assuming that the wind speed is not influenced by the surface roughness at this height), and Z_{om} (m) is the surface roughness length for the momentum transport (Campbell and Norman, 1998) which is defined mathematically as the plane where the wind speed becomes zero. The following equation has been suggested for customizing the function of Z_{om} based on NDVI (Allen *et al.*, 2007b):

$$z_{om} = \exp\left[(a * NDVI / \alpha) + b\right] \quad (19)$$

where α is the surface albedo which is used to differentiate between tall and short vegetation with the same NDVI, and andare the regression constants derived from a plot of $LN(Z_{om})$ versus $NDVI / \alpha$for two or more circumstances in the image for specific vegetation types. In this study, a regression line was developed based on $LN(z_{om})$ and NDVI values for two areas, a pistachio field and a bare-soil land. Due to being expensive and difficult to calculate, Z_{om} was estimated for the pistachio crop according to the results of the study by Yang and Friedi (2003) and the model presented by Choudhury and Monteith (1988). This model is relatively simple and its results are close to those of the study conducted by Yang and Friedi (2003). In addition, Z_{om} was set to 0.005 for bare soil (Gowda *et al.*, 2008) at NDVI of 0.09. The following is Eq. 18 where $u_{200}$is to consider as:

$$u_{200} = \frac{u_s * \ln(200 / zom_s)}{\ln(z_x / zom_{s)}} \quad (20)$$

Herein, u_s is the wind speed at the weather station at Z_x height above the surface, z_{oms} is the surface roughness for momentum transport at the weather station.

The corrected value for is calculated using an iterative procedure:

$$u^* = \frac{U_{200} K}{\ln(200 / z_{om}) - \psi_{m200}} \quad (21)$$

where ψ_{m200} is the stability correction for momentum transport at 200 m as:

$$r_{ah} = \frac{LN(z_2 / z_1) - \psi_{h(z2)} + \psi_{h(z1)}}{u^* \times K} \quad (22)$$

where $\psi_{h(z2)}$ and $\psi_{h(z1)}$ are the stability correction for heat transport at Z_1 and Z_2 heights. The atmospheric stability condition is defined by using Monin-Obukhov length L (m) and an iterative procedure. L is defined as:

$$L = -\frac{\rho_{air} C_p (u^*)^3 T_s}{KgH} \quad (23)$$

where L (m) is the stability condition of the atmosphere (that is determined iteratively), g is the earth gravity (ms^{-1}), $\rho$is the air density kgm^{-3} , is C_p the air specific heat at a constant pressure, Ts is the surface temperature (K), and u^* is the friction velocity (ms^{-1}). Then, the integrated stability correction values for momentum heat transfer (ψ_m and ψ_h) are calculated by following the method presented by Webb (1970) and Paulson (1970). For the details of the iteration procedure of stability correction, this study has followed Allen, et al. (2007b) and Bastiaanssen et al. (2002).

The temperature difference, dT, for each pixel was calculated by assuming a linear relationship between dT and Ts estimated from the satellite image thermal band (Allen *et al.*, 2007b).

$$dT = a + bT_S \quad (24)$$

The initial a and b values were used to correct the iterative stability. This was programmed on a Microsoft excel sheet. Through an excel program, the estimated values were then transferred to an ILWIS software to apply to all the pixels.This is how a and b were determined iteratively using twodTvalues and their associated T_S values from hot and cold pixels. METRIC and SEBAL follow the same approach in selecting hot pixels, but METRIC differs from SEBAL in selecting cold pixels. In SEBAL approach, cold pixels are selected in well-irrigated agricultural fields whereas, in METRIC, these pixels are selected from a tall reference grass field. In the absence of tall grass in the image scene, cold pixels are selected from a fully vegetated area

(LAI>4) by assuming that they have a LE value 1.05 times as much as expected for a tall reference crop (Tasumi *et al.*, 2005a). Therefore, LE of cold pixels is set to 1.05 times more than that of reference tall grass by assuming that these pixels have an ET rate 5% higher than that of reference grass (Allen *et al.*, 2007b). A hot pixel is a dry bare agricultural field where LE is assumed to be 0. This pixel has a relatively higher temperature and lower net radiation. Consequently, two extremes, namely hot and cold pixels, are selected within the image. These two pixels tie the calculations for all other pixels between these two points (Allen *et al.*, 2005).

$$dT_{hot} = \frac{(R_n - G) r_{ah-hot}}{\rho_{hot} C_p} \quad (25)$$

$$dT_{cold} = \frac{(R_n - G - kET_{ref}) r_{ah-cold}}{\rho_{cold} C_p} \quad (26)$$

where ET_{ref} is the hourly reference of ET that is proposed to be estimated from the standardized ASCE Penman–Monteith equation for alfalfa reference (ASCE-EWRI, 2004), is an empirical value and is set to 1.05 by assuming a 5% greater ET ET_{ref} than the in selected fields due to higher surface wetness as compared to other vegetation fields, r_{ah} is the aerodynamic resistance for heat transfer calculated for the hot and cold pixels, ρ is the air density, kgm^{-3} and C_p is the air specific temperature at a constant pressure. Consequently, H_{cold} and H_{hot} can be defined with regard to Equation 16 as the following:

$$H_{hot} = (R_n - G)_{hot} - LE_{hot} \quad (27)$$

$$H_{cold} = (R_n - G)_{cold} - LE_{cold} \quad (28)$$

Once R_n, H, and G have been calculated, Eq. 5 is used to estimate LE as the residual of surface energy balance. Finally, LE is divided by the latent heat of vaporization to estimate the instantaneous ET at the satellite overpass time (Allen *et al.*, 2007a):

$$ET_{ins} = 3600 \frac{\lambda E}{\gamma \rho_w} \quad (29)$$

in which ET_{ins} is the instantaneous ET (mmh^{-1}), 3600 converts from seconds into hours, ρ_w is the density of water (1,000 kgm^{-3}), and γ is the latent heat of vaporization Jkg^{-1} that is computed as follows:

$$\gamma = (2.501 - 0.00236(T_s - 273.15)) * 10^6 \quad (30)$$

In order to convert hourly ET to a daily basis, a reference ET fraction is computed through dividing ET_{ins} by calculated from the standardized ASCE Penman–Monteith equation.

$$ET_{ref} f = \frac{ET_{ins}}{ET_{ref}} \quad (31)$$

Finally, the actual 24-hour ET is estimated using $ET_{ref} f$ and the accumulated hourly ET reference obtained in the standardized ASCE Penman–Monteith method, assuming instantaneous $ET_{ref} f$ at the satellite overpass time is the same as the average $ET_{ref} f$ over 24 hours (Allen *et al.*, 2007a):

$$ET_{daily} = ET_{ref} f \sum_{i=1}^{24} ET_{ref(i)} \quad (32)$$

where $\sum_{i=1}^{24} ET_{ref(i)}$ accumulates the hourly for $ET_{ref} f$ 24 hours.

The METRIC inputs in this study were divided into two sets of variables. The first set consisted of primary inputs that were calculated from the image spectral bands or measured at the ground station. The second set included intermediate inputs calculated directly or indirectly from the primary input data. The input variables and their values are shown in Table 1. The METRIC-based ET sensitivity to the input parameters was analyzed by calculating ET at each step change of an input variable from the base case toward its upper limit and its lower limit by using the Sensitivity Analysis Add-In module of SensIt®. It should be noted that, in this analysis, the steps of change of values were based on the range of each variable. Consequently, the change step of a variable with a higher range was set to a higher step value. During the analysis, other variables were fixed to the base-case values shown in Table 1. In the study area, three dominant categories were chosen for sensitivity analysis. These categories with different values of LAI (LAI 1=2.8, LAI2=3.2 and LAI3=4.5) will be called LL1, LL2 and LL3 from now on. The values of the variables (inputs) at each chosen point were considered as the base cases, and the upper and lower limits of the input values were set to the maximum and minimum values of input maps. The incoming solar radiation value, measured in the weather station at the satellite overpass time, was set to 890 Wm^{-2}.

RESULTS & DISCUSSION

The ET map of the study area estimated by METRIC energy balance method is shown in Fig. 2.

Table 1. primary and intermediate parameters with their corresponding base case, lower limit and upper limit values at three level of LAI in sensitivity analysis

	Input Variable	Base Case			Lower limit	Upper limit
		LL1	LL2	LL3		
Primary	WS	1.0	1.0	1.0	0.5	4.0
	α	0.258	0.253	0.245	0.210	0.37
	NDVI	0.144	0.25	0.42	0.002	0.53
	SAVI	0.100	0.2	0.35	0.001	0.47
	LAI	2.8	3.2	4.5	0	6.2
Intermediate	Ts	324.3	319.9	315.7	311.2	329.5
	Air T	40.60	40.60	40.60	20.0	42.00
	dT	16.73	5.668	0.001	0.001	29.8
	H	330.8	114.9	0.011	0.006	539.8
	Rn	614.8	649.7	688.1	474.2	754.4
	G	139.6	132.5	123.6	113.4	144.1
	u^*	0.194	0.206	0.135	0.098	0.249
	r_{ah}	56.86	55.45	101.6	20.16	166.6
	Z_{om}	0.042	0.087	0.127	0.005	0.246
	ε_o	0.92	0.94	0.957	0.92	0.986

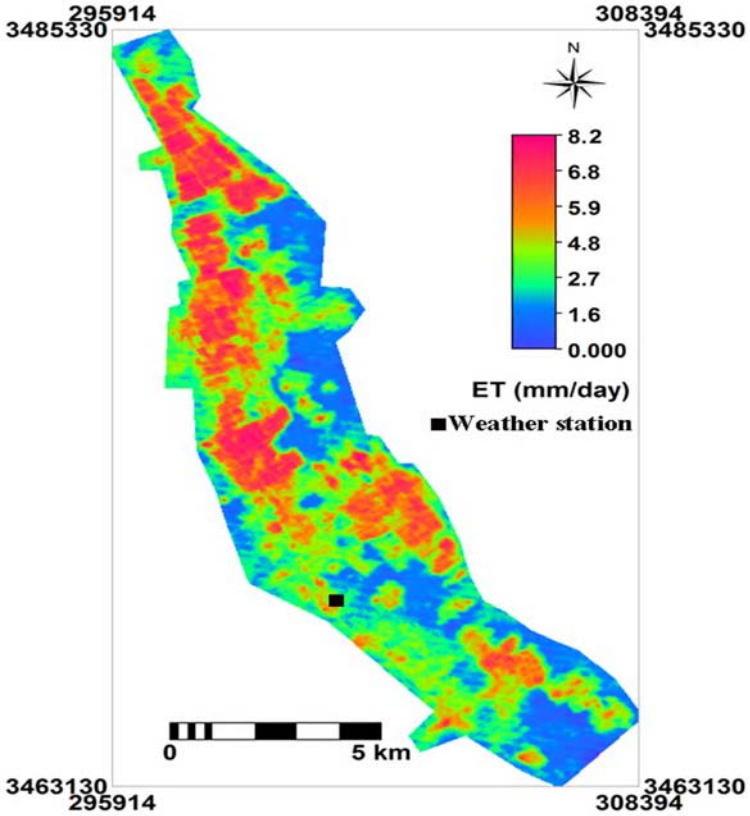

July 17

Fig. 2. ET map and the location of weather station

Surface temperature (Ts) is the most important input parameter with the steepest slop in this graph. Ts was identified as the most important parameter also by previous studies (Timmermans *et al.*, 2007; Wang *et al.*, 2009; Long *et al.*, 2011). A one-percent change in Ts lead to a 1.6 mm day^{-1} ET change. The next effective parameter is surface albedo (α). Areas with a higher albedo value have an increased outgoing shortwave radiation and, consequently, the available Rn is decreased in these areas. The accuracy of albedo estimation depends on the accurate estimate of the surface reflectance in visible near infrared and shortwave bands. A one percent change in the surface albedo causes a 0.056 mm day^{-1} ET. Albedo was examined as the intermediate parameter in the study by Wang et al. (2009). However, they also recognized albedo as the next sensitive parameter. The third sensitive parameter is air temperature in which a one-percent change leads to a 0.02 mm day^{-1} ET change. Air temperature is used to calculate incoming long-wave radiation (Eq.10). The effect of this parameter on ET has not been evaluated in previous studies. A summary of the primary input sensitivity analysis is given as graphs in Fig. 3. In order to a better visualization of the lines in Fig. 3, only the starting and the ending points are highlighted, and the mid points are kept as small as possible. Because of similar trends of primary input at three different tested locations, the graph of LL3 point has been presented in this study. NDVI, SAVI, LAI, and wind speed are located along almost the same line. The relationship of these parameters and ET has been presented in Table 2. The observed variations have a slight influence on the METRIC output. Unlike, Wang et al. (2009) reported that wind speed is one of the most influential parameter within the primary input variables. However, previous studies used different reference (base), upper limit and lower limit of input variables for evaluating the ET (Wang *et al.*, 2009; Timmermans *et al.*, 2007; Long *et al.*, 2011). Therefore, the selected various reference points make direct comparison of the different studies difficult. In the present study the values at three dominant categories were chosen as the base and consequently the lower and upper limits were set to the minimum and maximum values of the image respectively. For the ground-based inputs parameters (eg. Wind speed), the study used the satellite overpass time value and minimum and maximum values which normally occurs in the study area as the base, lower and upper limit respectively. NDVI may be used to calculate many other parameters in the METRIC algorithm such as surface emissivity (Eq. 9), SAVI (Eq. 13), Z_{om} (Eq. 19), LAI (Eq. 12), and G (Eq. 14). Consequently, ET is indirectly affected by NDVI via other primary and intermediate parameters. According to these findings, an accurate estimation of NDVI from the reflectance values of visible-near infrared bands seems to be necessary. In this study, LAI was used to calculate surface emissivity. However, as it can be seen in Fig. 3, the effect of LAI on ET was found to be little, especially in areas with a relatively good vegetation cover. This has also been stated by Allen et al. (2007b). In this study, a two-factor analysis of the primary inputs which has not been evaluated in the previous studied was performed. The results are shown in Figs. 4, 5, and 6 for the three samples LL3, LL2, and LL1

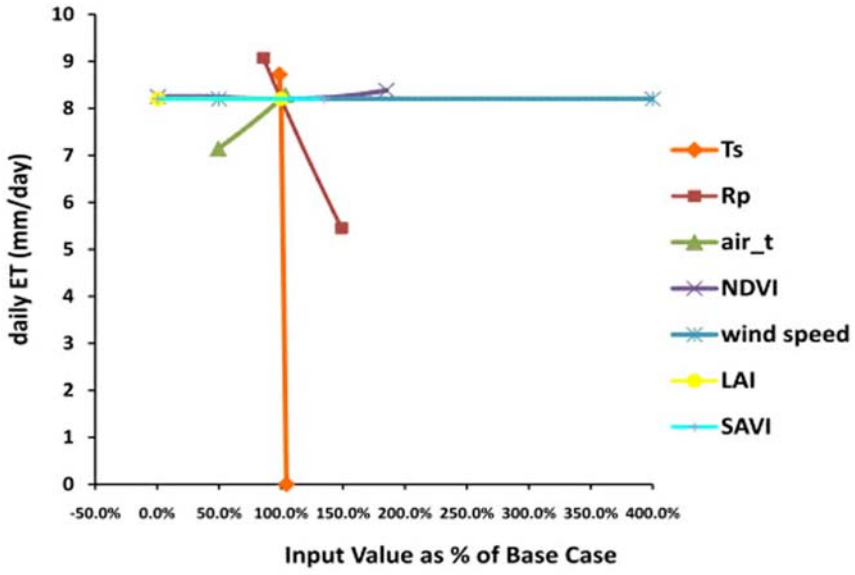

Fig. 3. Graph showing the sensitivity of METRIC to the primary inputs

Table 2. Relationship between primary input parameters and ET, "x" presents input variables in percentage

Input parameter	Equation	R^2	Type
Surface temperature	y = -159.02x + 166.22	0.9659	Linear
Surface Albedo	y = -5.7168x + 13.931	0.9995	Linear
Air Temperature	y = 2.1063x + 6.0873	0.9992	Linear
NDVI	$y = 0.1358x^2 - 0.2139x + 8.289$	0.8583	Polynomial order 2
Wind speed	y = -0.0002x + 8.2032	1	Linear
SAVI	y = 2E-14x + 8.2031	2E-15	Linear
LAI	y =- 0.0001x + 8.2032	0.9684	Linear

respectively. The paired numbers of paired input variables and their locations indicate the input variables and the vectors of ET swing (increase or decrease from the base) respectively. The albedo-Ts pair is the most influential parameter in the three sample sites where ET swings between 0 and 9.6 mm day^{-1} from its lower limit to its upper limit as given in Table 1. The next important paired parameter is NDV-Ts. By the change of its value, ET swings from 0 to 8.9 mm day^{-1}. The Ts-air temperature pair has the same effect as NDVI-Ts on ET swing. LAI-Ts, Ws-Ts, and SAVI-Ts pairs cause ET to swing between 0 and 8.7 mm day^{-1}. The other pairs of the primary inputs are ranked from top (the most influential pairs) to bottom (the least influential pairs) in Figs. 4, 5, and 6 referring to different sample sites. However, the order is changed from the 6th pair of the input at different sample locations. LAI-SAVI in LL3 site and NDVI-SAVI in both LL2 and LL1 locations are the least influential pairs in this analysis. The swing of ET due to the change in the other pairs of the input refers to the values of the corresponding sample sites in Figs 4, 5, and 6.

A summary of the sensitivity analysis of intermediate parameters is given in Fig. 7. Temperature gradient (dT) is a relative value calculated from the

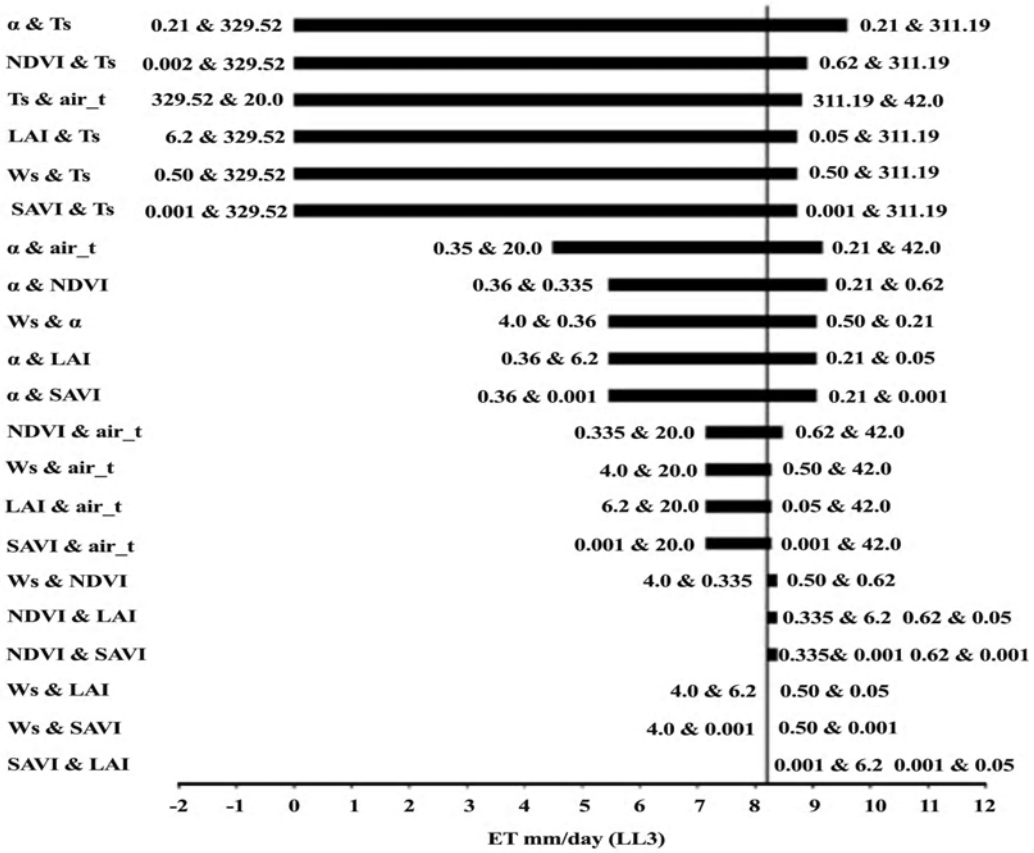

Fig. 4. Two-factor analysis of primary inputs at LL3

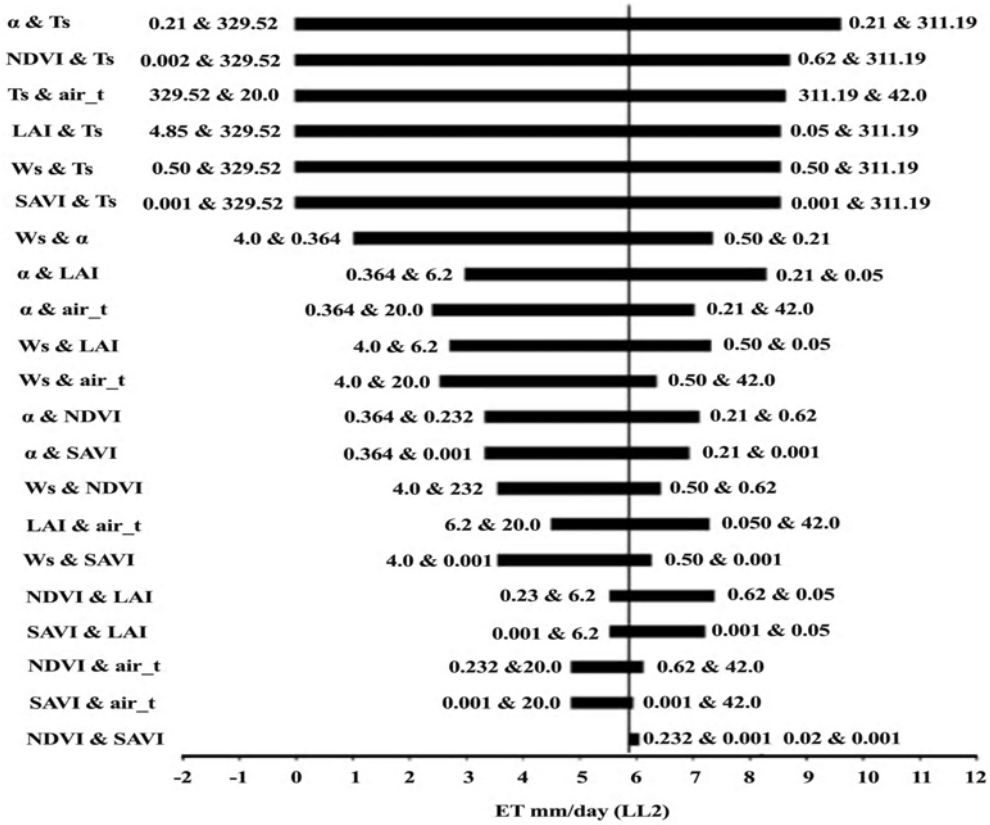

Fig. 5. Two-factor analysis of primary inputs at LL2

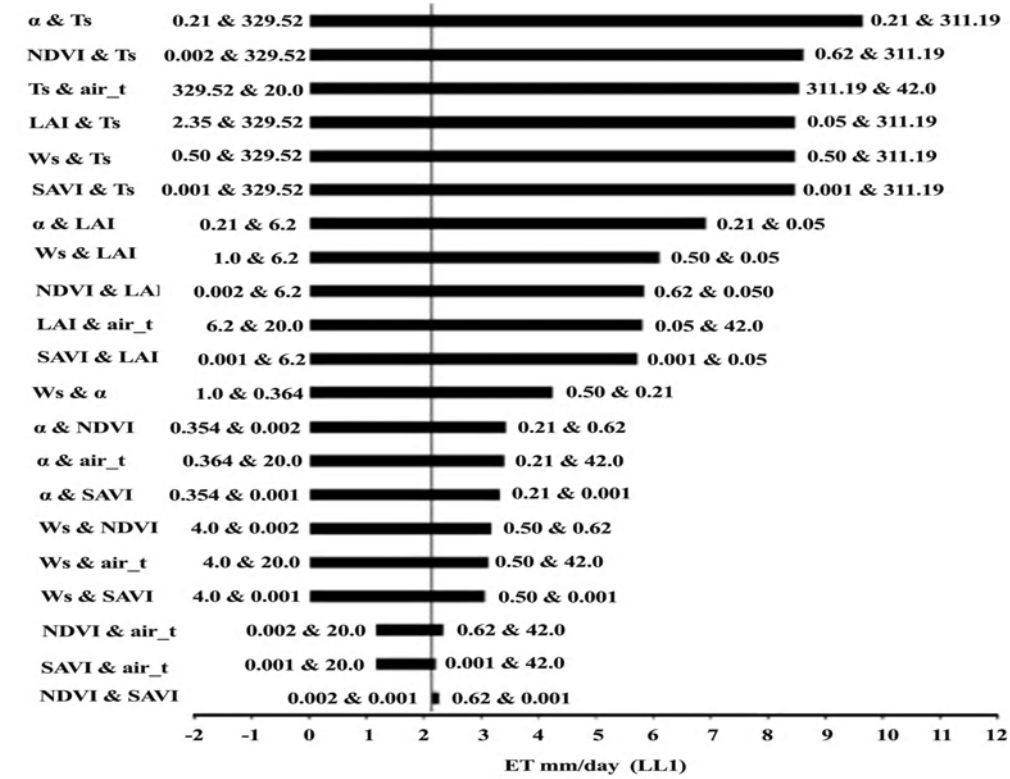

Fig. 6. Two-factor analysis of primary inputs at LL1

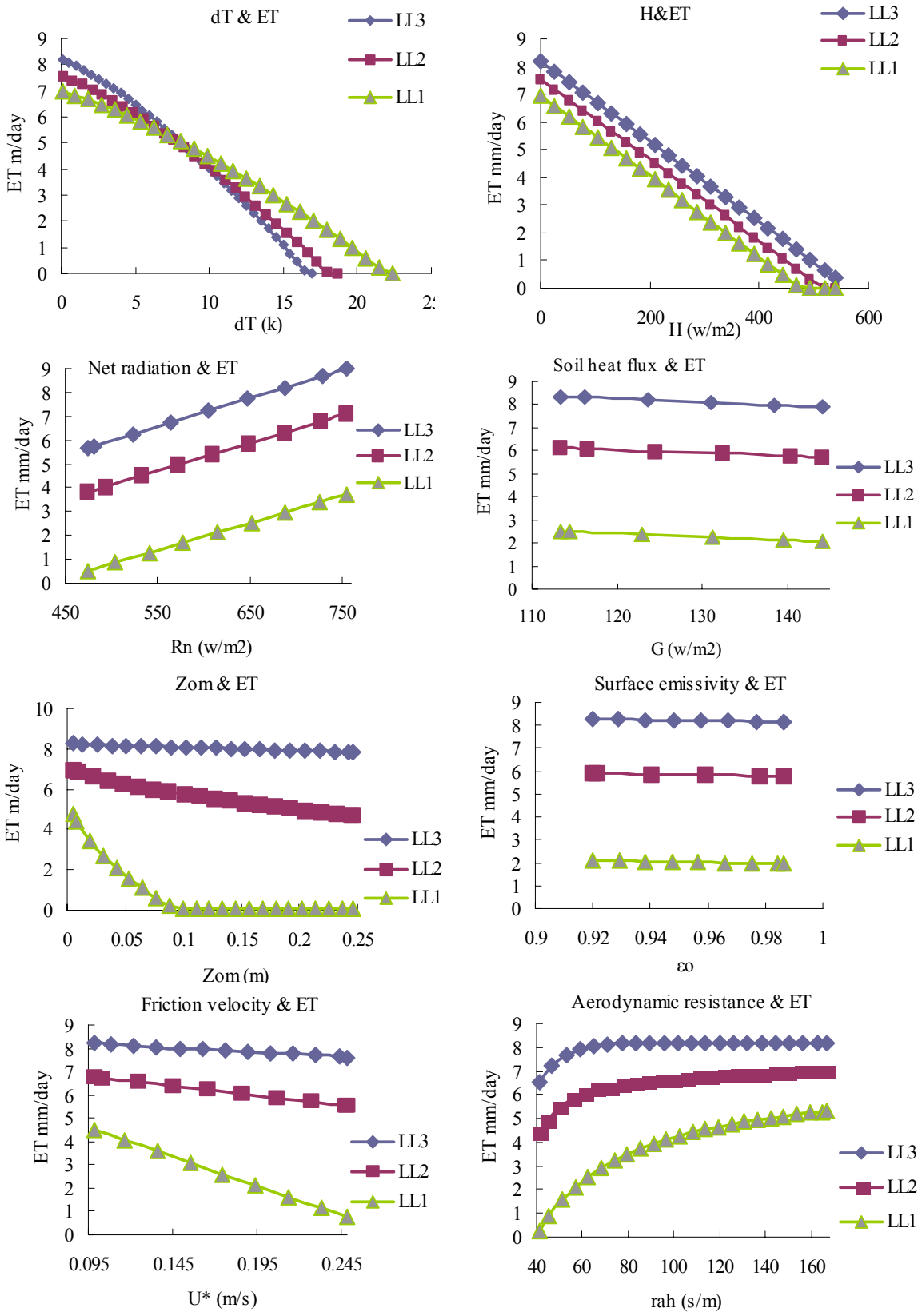

Fig. 7. Relationship of intermediate input parameters and ET estimate by METRIC

regression equation (linear function) of the values at the two extreme points of dry and wet pixels. Therefore, an accurate estimation of dT depends on the appropriate selection of these two extreme points, although, dT calculated from Ts is not affected by the error of Ts. This has also been concluded in the in the last studies (Wang *et al.,* 2009; Long *et al.,* 2011; Timmermans *et al.,* 2007). The results showed that a one-percent change of dT changes ET by 0.021 to 0.023 mm day^{-1}. The change rate varies at different levels of vegetation as shown in Fig. 7.

Also, a one-percent change of the sensible heat flux (H) (Eq. 16) from the base value can lead to a change of 0.23 mm day^{-1} in ET by METRIC. In the areas with low vegetation, energy is mostly dominated by H and vice versa. However, the same trends were followed by changing H at three different levels of LAI values. The accuracy of H depends on the accuracy of dT function generated from anchor points and the accuracy of estimated aerodynamic resistance to heat transfer. Friction velocity has proved to have different effects on ET at different levels of vegetation. It is a function of wind speed and Z_{om} (Eq. 19). As a result, it is increased by increasing wind speed. Wang et al. (2009) drew the same conclusions about H and sensitivity. The sensitivity of METRIC to is increased by decreasing LAI. The effects vary from 0.001 to 0.05 mm day^{-1} ET per a one-percent change in (see the equations in Table 3).

Apart from the above variables, a one-percent change in the net radiation (Rn) and the soil heat flux (G) causes a change in ET by 0.07 and 0.018 mm day^{-1} at all LAI values respectively. Besides, roughness length for momentum at high values of LAI does not make much difference in the ET resulted by METRIC. However, the rate is increased at the LL1 location (about 0.03 mm day^{-1} per a one-percent change at <0.1). Surface emissivity also plays an important role in determining the amount of outgoing long-wave radiation from the surface. The effect of on ET is about 0.018 to 0.023 mm day^{-1} that is decreased by increasing vegetation. Since the range of these values is small, the effect of this variable is slight. However, it is used to calculate surface temperature and outgoing long-wave radiation (Eqs. 4 and 8). The aerodynamic resistance to heat transfer (Eq. 17) influences ET by 0.01 to 0.05 mm day^{-1} per a one-percent change, and its effects vary at different levels of vegetation as it is seen in Fig. 7.

Table 3. Relationship between intermediate input parameter and ET, "x" presents input variables in percentage

Input parameter		Equation	R^2	Type
dT	LL1	y = -0.4041x2 - 1.8744x + 7.0609	0.9996	Polynomial order 2
	LL2	y = -0.3701x2 - 1.9395x + 7.6635	0.9992	Polynomial order 2
	LL3	y = -0.2618x2 - 1.613x + 8.3145	0.9997	Polynomial order 2
H		y = -0.2323x + 7.4818	0.9832	Linear
Rn		y = 6.9634x - 4.8483	1	Linear
G		y = -1.7953x + 9.9984	1	Linear
u^*	LL1	y = -4.8483x + 6.9634	1	Linear
	LL2	y = -1.6771x + 7.5466	1	Linear
	LL3	y= -0.0002x + 8.2032 x	1	Linear
r_{ah}	LL1	$y = 0.7265x^3 - 5.1904x^2 + 13.051x - 6.578$	0.998	Polynomial order 3
	LL2	$y = 0.628x^3 - 4.199x^2 + 9.367x - 0.1955$	0.9723	Polynomial order 3
	LL3	$y = 4.1876x^3 - 14.786x^2 + 16.74x + 2.1641$	0.9266	Polynomial order 3
Z_{om}	LL1	$y = -0.083x^3 + 1.032x^2 - 4.097x + 5.196$	0.996	Polynomial order 3
	LL2	$y = 0.131x^2 - 1.159x + 6.923$	0.995	Polynomial order 2
	LL3	y = -0.212x + 8.239	0.982	Linear
ε_o	LL1	y = -2.3258x + 4.4409	1	Linear
	LL2	y = -2.0717x + 7.9413	1	Linear
	LL3	y = -1.8199x + 10.023	1	Linear

CONCLUSION

METRIC-based ET is highly sensitive to Ts; therefore, an accurate estimation of surface temperature using satellite thermal bands and surface emissivity is necessary for an accurate estimation of ET. Nevertheless, dT is not affected by error in the estimation of surface temperature since dT is a relative value calculated from the values at two extreme anchor pixels on the image. Therefore, any inappropriate selection of wet and dry pixel in both SEBAL and METRIC is a major source of errors as stated by authors in some previous studies. Based on the results of the present study, METRIC is sensitive to dT whose sensitivity grows to dense vegetation. Also, ET is affected by surface albedo as a second influential parameter of primary inputs. Albedo can only be calculated from the reflectance values of visible-near infrared and the short wave bands of satellite data. The calculation is always followed on the order of image producer. Therefore, procedure is user-independent. METRIC is less sensitive to NDVI, SAVI, LAI, and the wind speed of primary inputs, although NDVI is an important parameter used to calculate several parameters in the algorithm. Thus, an accurate estimation of NDVI is a key parameter in the algorithm. The algorithm is highly sensitive to H so that a change of 1 percent in H leads to a 0.23 mm day^{-1} reduction in ET. The rate of ET change by Z_{om}, u^*, ε_o, and r_{ah} varies at different levels of vegetation. METRIC is moderately sensitive to , , and r_{ah} and less sensitive to (except for <0.1). Besides, ET is highly affected by G and Rn although the rate of ET change by Rn is higher than that by G. In conclusion, METRIC is highly sensitive to Ts, Rn, , , dT, H, and air temperature, moderately sensitive to G, r_{ah}, , and less sensitive to LAI, SAVI, wind speed, and. LE calculated as the residual energy in an energy budget equation accumulates the errors of Rn, G, and H components that can be additive or compensating. A two-factor sensitivity analysis also confirmed that the Ts and pair is the most and NDVI-SAVI and SAVI-LAI pairs are the least effective. These pairs of primary inputs swing ET by 9.6 and about 0.1 mm day-1 respectively. Thus, an accurate estimation of input parameters by focusing on the most influential parameters mentioned above reduces the error of LE and, as a result, the error in the ET estimate. METRIC uses an equation based on the ratio of the actual ET to the hourly calculated from the weather data (ASCE Penman Monteith method) for converting ET from an hourly value to a daily basis or longer time bases. The accuracy of has been proved in previous studies. However, the ratio-based equation does not strongly affect ET to convert it to a daily basis as a short-time one. Nevertheless, it has been reported that seasonal METRIC ET (that utilizes reference ET for interpolation/extrapolations) is overestimated compared to that of flux measurements (Tang *et al.*, 2009). In order to improve the accuracy of the algorithm, this study suggests to improve equations of high impact on the above variables. Also, according to the previous studies, the efficiency of non linear dT function needs to be assessed.

ACKNOWLEDGEMENT

We acknowledge the technical support and the facilities provided by the agricultural organization of the city of Yazd for field soil-water data collection. We also would like to thank the University of Idaho for providing REF-ET software that has been used in this study for calculation reference ET.

REFERENCES

Allen, R., Tasumi, M., Morse, A. and Trezza, R. (2005). A Landsat-based energy balance and evapotranspiration model in Western US water rights regulation and planning. Irrigation and Drainage Systems, **19** (**3**), 251-268.

Allen, R. G. and Bastiaanssen, W. G. M. (2005). Special issue on remote sensing of crop evapotranspiration for large regions. Irrigation and Drainage Systems, **19**, 207-210.

Allen, R. G., Tasumi, M., Morse, A., Trezza, R., Wright, J. L., Bastiaanssen, W., Kramber, W., Lorite, I. and Robison, C. W. (2007a). Satellite-Based Energy Balance for Mapping Evapotranspiration with Internalized Calibration (METRIC)—Applications. J. Irrig. Drain Eng., **133** (**4**), 395-406.

Allen, R. G., Tasumi, M. and Trezza, R. (2007b). Satellite-Based Energy Balance for Mapping Evapotranspiration with Internalized Calibration (METRIC) Model. J. Irrig. Drain Eng., **133** (**4**), 380-394.

ASCE-EWRI, (2004). The ASCE standardized reference evapotranspiration equation. Environmental and Water Resources Institute of the ASCE, Report by the Task Committee on Standardization of Reference Evapotranspiration.

Bastiaanssen, W. G. M. (1995). Regionalization of surface flux densities and moisture indicators in composite terrain. A remote sensing approach under clear skies in Mediterranean climates., Dissertation, 273 Wageningen: Agricultural University of Wageningen.

Bastiaanssen, W. G. M. (2000). SEBAL-based sensible and latent heat fluxes in the irrigated Gediz Basin, Turkey. J. Hydrol., **229**, 87-100.

Bastiaanssen, W. G. M., Allen, R., Ralf, W., Tasumi, M. and Trezza, R. (2002). SEBAL advance training and user manual. 39 Idaho.

Bastiaanssen, W. G. M., Menenti, M., Feddes, R. A. and Holtslag, A. A. M. (1998). A remote sensing surface energy

balance algorithm for land (SEBAL): 1. Formulation. J. Hydrol., **212-213** (**1-4**), 198-212.

Bastiaanssen, W. G. M., Noordman, E. J. M., Pelgrum, H., Davids, G., Thoreson, B. P. and Allen, R. G. (2005). SEBAL model with remotely sensed data to improve water-resources management under actual field conditions. J. Irrig. Drain Eng., **131** (**1**), 85-93.

Brutsaert, W. (Eds) (1982). Evaporation into the Atmosphere: Theory, History and Applications. Boston Kluwer Academic.

Campbell, G. S. and Norman, J. M. (Eds) (1998). An Introduction to Environmental Biophysics. Springer; 2nd edition.

Chander, G. and Markham, B. (2003). Revised Landsat-5 TM radiometric calibration procedures and postcalibration dynamic ranges. IEEE Transactions On Geoscience And Remote Sensing, **41 (11)**, 2674-2677.

Chavez, J. L., Gowda, P. H., Howell, T. A. and Copeland, K. S. (2009). Radiometric surface temperature calibration effects on satellite based evapotranspiration estimation. Int. J. Remote Sens., **30** (**9**), 2337 - 2354.

Chavez, J. L., Gowda, P. H., Howell, T. A., Marek, T. H. and New, L. L. (2007).Evapotranspiration mapping using METRIC™ for a region with highly advective conditions. In 2007 ASABE Annual International Meeting, Technical Papers, Vol. 4 BOOK.

Chavez, P. S. J. (1988). An improved dark-object subtraction technique for atmospheric scattering correction of multispectral data. Remote Sens. Environ., **24** (**3**), 459-479.

Choi, M., Kustas, W. P., Anderson, M. C., Allen, R. G., Li, F. and Kjaersgaard, J. H. (2009). An intercomparison of three remote sensing-based surface energy balance algorithms over a corn and soybean production region (Iowa, U.S.) during SMACEX. Agr. Forest Meteorol. **149** (**12**), 2082-2097.

Choudhury, B. J. and Monteith, J. L. (1988). A four-layer model for the heat budget of homogeneous land surfaces. Q. J. Roy. Meteor. Soc., **114** (**480**), 373-398.

Conrad, C., Dech, S., Hafeez, M., Lamers, J., Martius, C. and Strunz, G. (2007). Mapping and assessing water use in a Central Asian irrigation system by utilizing MODIS remote sensing products. Irrigation and Drainage Systems, **21** (**3**), 197-218.

Ferrari, G., Mondéjar-Jiménez, J. and Vargas - Vargas, M. (2010). Environmental Sustainable Management of Small Rural Tourist Enterprises. Int. J. Environ. Res., **4** (**3**), 407-414.

Folhes, M. T., Rennó, C. D. and Soares, J. V. (2009). Remote sensing for irrigation water management in the semi-arid Northeast of Brazil. Agr. Water Manage., **96** (**10**), 1398-1408.

Gowda, P., Chavez, J., Howell, T., Marek, T. and New, L. (2008). Surface Energy Balance Based Evapotranspiration Mapping in the Texas High Plains. Sensors, **8** (**8**), 5186-5201.

Hendrickx, J. M. H., Kleissl, J., Velez, J. D. G., Hong, S.-h., Duque, J. R. F., Vega, D., Ramirez, H. A. M. and Ogden, F. L. (2007). Scintillometer networks for calibration and validation of energy balance and soil moisture remote sensing algorithms. In Algorithms and Technologies for Multispectral, Hyperspectral, and Ultraspectral Imagery XIII, Vol. 6565, 65650W-65616 Orlando, FL, USA: SPIE.

Irmak, A. and Kamble, B. (2009). Evapotranspiration data assimilation with genetic algorithms and SWAP model for on-demand irrigation. Irrigation Sci., **28** (**1**), 101-112.

Lin, M. L., Chu, C. M. and Tsai, B. W. (2011). Drought Risk Assessment in Western Inner-Mongolia. Int. J. Environ. Res., **5** (**1**), 139-148.

Long, D., Singh, V. P. and Li, Z.-L. (2011). How sensitive is SEBAL to changes in input variables, domain size and satellite sensor? J. Geophys. Res., **116**, D21107, doi:10.1029/2011JD016542.

Markham, B. L. and Barker, J. L. (1986). Landsat MSS and TM post calibration dynamic ranges, exoatmospheric reflectances and at-satellite temperatures, EOSAT Landsat Technical Notes, **1**, 3-8.

Mondéjar-Jiménez, J. A., Cordente-Rodríguez, M., Meseguer-Santamaría, M. L. and Gázquez-Abad, J. C. (2011). Environmental Behavior and Water Saving in Spanish Housing. Int. J. Environ. Res., **5** (**1**), 1-10.

Nakane, K. and Haidary, A. (2010). Sensitivity Analysis of Stream Water Quality and Land Cover Linkage Models Using Monte Carlo Method. Int. J. Environ. Res., **4** (**1**), 121-130.

Paulson, C. A. (1970). The mathematical representation of wind speed and temperature profiles in the unstable atmospheric surface layer. J. Appl. Meteorol., **9**, 857-861.

Ramos, J. G., Cratchley, C. R., Kay, J. A., Casterad, M. A., Martínez-Cob, A. and Domínguez, R. (2009). Evaluation of satellite evapotranspiration estimates using ground-meteorological data available for the Flumen District into the Ebro Valley of N.E. Spain. Agr. Water Manage., **96** (**4**), 638-652.

Tang, Q., Peterson, S., Cuenca, R. H., Hagimoto, Y. and Lettenmaier, D. P. (2009). Satellite-based near-real-time estimation of irrigated crop water consumption. J. Geophys. Res., **114,** D05114.
doi:10.1029/2008JD010854

Tasumi, M. (2003). Progress in operational estimation of regional evapotranspiration using satellite imagery. Dissertation, 357 Idaho: University of Idaho.

Tasumi, M., Allen, R. G. and Trezza, R. (2007). Estimation of at surface reflectance and albedo from satellite for routine, operational calculation of land surface energy balance. journal of hydrologic engineering.

Tasumi, M., Allen, R. G., Trezza, R. and Wright, J. L. (2005a). Satellite-based energy balance to assess within-population variance of crop coefficient curves. J. Irrig. Drain Eng., **131** (**1**), 94-109.

Tasumi, M., Trezza, R., Allen, R. and Wright, J. (2005b). Operational aspects of satellite-based energy balance models for irrigated crops in the semi-arid U.S. Irrigation and Drainage Systems, **19** (**3**), 355-376.

Timmermans, W. J., Kustas, W. P., Anderson, M. C. and French, A. N. (2007). An intercomparison of the Surface Energy Balance Algorithm for Land (SEBAL) and the Two-Source Energy Balance (TSEB) modeling schemes. Remote Sens. Environ., **108** (**4**), 369-384.

Trezza, R. (2006). Estimation Of Evapotranspiration From Satellite-Based Surface Energy Balance Models For Water Management in the Rio Guarico irrigation system, Venezuela. In Earth Observation For Vegetation Monitoring and Water Management, **852** (**1**), 162-169 (Paper presented at the AIP, Naples Italy).

Walter, I. A., Allen, R. G., Elliott, I., R. , Brown, M. E., Jensen, D. P., Mecham, B., Howell, T. A., Snyder, R., Eching, S., Spofford, T., Hattendorf, M., Martin, D., Cuenca, R. H. and Wright, J. L. (2002). ASCE, Standardized Reference Evapotranspiration Equation.

Wang, J., Sammis, T. W., Gutschick, V. P., Gebremichael, M. and Miller, D. R. (2009). Sensitivity Analysis of the Surface Energy Balance Algorithm for Land (SEBAL). Transactions of the ASABE, **52** (**3**), 801-811.

Webb, E. K. (1970). Profile relationships: the log-linear range, and extension to strong stability. Quart. J. Roy. Meteorol. Soc., **96**, 67-90.

Yang, R. and Friedl, M. A. (2003). Determination of Roughness Lengths for Heat and Momentum Over Boreal Forests. Bound-Lay. Meteorol., **107** (**3**), 581-603.